NeuroImage: Clinical 12 (2016) 976–989

Contents lists available at ScienceDirect

NeuroImage: Clinical

journal homepage: www.elsevier.com/locate/ynicl

Combined ^{18}F-FDG-PET and diffusion tensor imaging in mesial temporal lobe epilepsy with hippocampal sclerosis

Javier Aparicio[a,*], Mar Carreño[a,f], Núria Bargalló[b,f], Xavier Setoain[c,f], Sebastià Rubí[g], Jordi Rumià[d], Carles Falcón[e], Anna Calvo[f], Berta Martí-Fuster[h,i], Nelly Padilla[j], Teresa Boget[f,l], Luís Pintor[f,k], Antonio Donaire[a,f]

[a]Hospital Clínic, Epilepsy Program, Department of Neurology, Neuroscience Institute, CP 08036, Barcelona, Spain
[b]Hospital Clínic, Epilepsy Program, Department of Radiology, CDIC, CP 08036, Barcelona, Spain
[c]Hospital Clínic, Epilepsy Program, Department of Nuclear Medicine, CDIC, CP 08036, Barcelona, Spain
[d]Hospital Clínic, Epilepsy Program, Department of Neurosurgery, Neuroscience Institute, CP 08036, Barcelona, Spain
[e]BarcelonaBeta Brain Research Center, Pasqual Maragall Foundation, CP 08003, Barcelona, Spain
[f]Institut d'investigacions Biomèdiques August Pi i Sunyer (IDIBAPS), CP 08036, Barcelona, Spain
[g]Nuclear Medicine Department, Hospital Universitari Son Espases, Instituto de Investigación Sanitaria de Palma, CP 07010, Palma, Spain
[h]Grupo de Imagen Biomédica de la Universidad de Barcelona (GIB-UB), Biomedical Research Networking Center in Bioengineering, Biomaterials and Nanomedicine (CIBER-BBN), CP 08036, Barcelona, Spain
[i]Department of Physiological Sciences I - Biophysics and Bioengineering Unit, University of Barcelona, CP, 08036, Barcelona, Spain
[j]Department of Women's and Children's Health, Karolinska Institutet, Stockholm, Sweden
[k]Hospital Clínic, Epilepsy Program, Department of Psychiatry, Neuroscience Institute, CP 08036, Barcelona, Spain
[l]Hospital Clínic, Epilepsy Program, Department of Neuropsychology, Neuroscience Institute, CP 08036, Barcelona, Spain

ARTICLE INFO

Article history:
Received 11 November 2015
Received in revised form 29 April 2016
Accepted 5 May 2016
Available online 6 May 2016

Keywords:
Positron emission tomography
DTI
MTLE
Hippocampus
Nerve net

ABSTRACT

Objectives: Several studies using ^{18}F-fluorodeoxyglucose positron emission tomography (^{18}F-FDG-PET) or diffusion tensor imaging (DTI) have found both temporal and extratemporal abnormalities in patients with mesial temporal lobe epilepsy with ipsilateral hippocampal sclerosis (MTLE-HS), but data are lacking about the findings of both techniques in the same patients. We aimed to determine whether the extent of ^{18}F-FDG-PET hypometabolism is related to DTI abnormalities.
Methods: Twenty-one patients with MTLE-HS underwent comprehensive preoperative evaluation; 18 (86%) of these underwent epilepsy surgery. We analyzed and compared the pattern of white matter (WM) alterations on DTI and cortical hypometabolism on ^{18}F-FDG-PET.
Results: We found widespread temporal and extratemporal ^{18}F-FDG-PET and DTI abnormalities. Patterns of WM abnormalities and cortical glucose hypometabolism involved similar brain regions, being more extensive in the left than the right MTLE-HS. We classified patients into three groups according to temporal ^{18}F-FDG-PET patterns: hypometabolism restricted to the anterior third (n = 7), hypometabolism extending to the middle third (n = 7), and hypometabolism extending to the posterior third (n = 7). Patients with anterior temporal hypometabolism showed DTI abnormalities in anterior association and commissural tracts while patients with posterior hypometabolism showed WM alterations in anterior and posterior tracts.
Conclusions: Patients with MTLE-HS have widespread metabolic and microstructural abnormalities that involve similar regions. The distribution patterns of these gray and white matter abnormalities differ between patients with left or right MTLE, but also with the extent of the ^{18}F-FDG-PET hypometabolism along the epileptogenic temporal lobe. These findings suggest a variable network involvement among patients with MTLE-HS.

1. Introduction

Mesial temporal lobe epilepsy (MTLE) is the most common form of intractable epilepsy in adults. MTLE is usually associated with ipsilateral hippocampal sclerosis (HS). MTLE-HS surgery leads to long-term seizure freedom in only about 60% of patients (Hemb et al., 2013). These results suggest that there may be distinct underlying neural substrates associated with seizure generation in a substantial subgroup of MTLE patients (Bonilha et al., 2012). They also show evidence that

* Corresponding author at: Epilepsy Program, Department of Neurology, Institute of Neuroscience, Hospital Clínic, C/Villarroel 170, CP 08036, Barcelona, Spain.
E-mail addresses: japaricio80@gmail.com, japarici@clinic.ub.es (J. Aparicio), mcarreno@clinic.ub.es (M. Carreño), bargallo@clinic.ub.es (N. Bargalló), setoain@clinic.ub.es (X. Setoain), s.rubi.sureda@gmail.com (S. Rubí), jrumia@clinic.ub.es (J. Rumià), cfalcon@fpmaragall.org (C. Falcón), anna.calvo@idibaps.org (A. Calvo), bertins98@gmail.com (B. Martí-Fuster), nelly.padilla@ki.se (N. Padilla), tboget@clinic.ub.es (T. Boget), lpintor@clinic.ub.es (L. Pintor), jdonaire@clinic.ub.es (A. Donaire).

http://dx.doi.org/10.1016/j.nicl.2016.05.002

conventional electrophysiological and neuroimaging techniques sometimes fail to infer the location and/or the extension of the epileptogenic zone (EZ) (Bonilha et al., 2007). In this context, neuroimaging techniques such as ^{18}F-fluorodeoxyglucose positron emission tomography (^{18}F-FDG-PET) and diffusion tensor imaging (DTI) can provide further insight into the pathophysiology of MTLE-HS.

In MTLE, ^{18}F-FDG-PET helps to identify the epileptogenic temporal lobe in 70% to 90% of patients (Kim et al., 2003). However, the hypometabolism depicted by ^{18}F-FDG-PET is typically larger than the presumed EZ and sometimes extends to remote extratemporal regions anatomically connected with mesial temporal structures (Wong et al., 2010). Extratemporal hypometabolism in MTLE-HS could result from the propagation of the epileptic activity from the temporal focus through the epileptic network (Chassoux et al., 2004; Takaya et al., 2006). It may reflect physiological dysfunction of the underlying temporal lobe and functionally associated regions (Vielhaber et al., 2003).

On the other hand, DTI can indirectly evaluate microstructural changes in the white matter (WM), thus allowing the integrity of WM tracts to be assessed (Basser and Pierpaoli, 1996). DTI findings in MTLE-HS include decreased fractional anisotropy (FA) and increased mean diffusivity (MD) in the temporal lobe (Gross, 2011). However, these changes are not confined to the involved temporal lobe, but rather involve an extensive bilateral temporal and extratemporal network of WM structures. WM alterations in DTI have been described in the frontal lobe, parieto-occipital cortices, corpus callosum and cingulum (Ahmadi et al., 2009; Concha et al., 2009; Concha et al., 2005; Focke et al., 2008; Gross, 2011; Gross et al., 2006; Lin et al., 2008; McDonald et al., 2008; Otte et al., 2012). It is unclear whether the WM diffusivity changes topographically coincide with cortical hypometabolism observed in ^{18}F-FDG-PET in MTLE.

We hypothesized that ^{18}F-FDG-PET and DTI could provide complementary information. Both techniques could reflect two basic aspects of the pathophysiological changes (epileptic network) related to the MTLE: the metabolic cortical dysfunction (^{18}F-FDG-PET) and the subcortical WM microstructural abnormalities (DTI) related to the generation and propagation of the epileptic activity. In this study, to better understand the regional extent of the metabolic and microstructural abnormalities in MTLE, we explored spatial relationship between ^{18}F-FDG-PET and DTI findings in a homogeneous group of patients with MTLE-HS. Our aims were (i) to describe the extent of the metabolic abnormalities found in patients with MTLE-HS in ^{18}F-FDG-PET; (ii) to study the microstructural changes across the WM of the entire brain; and (iii) to compare the pattern of WM alterations in DTI and cortical glucose hypometabolism in ^{18}F-FDG-PET. Single-subject and group-level voxel-based analyses of ^{18}F-FDG-PET and DTI data were applied.

2. Materials & methods

2.1. Subjects

The study population included 21 patients (13 women, mean age 36.14 years ± 10.79, range 18 to 60 years) with MTLE-HS admitted to our epilepsy unit for presurgical evaluation between 2009 and 2011 (See Table 1). All the patients underwent long-term video-EEG monitoring, 3T magnetic resonance imaging with a specific epilepsy protocol, DTI, and ^{18}F-FDG-PET. To be included in the study patients should have evidence of unilateral HS on MRI. Also, the seizure semiology and the ictal EEG pattern should be consistent with MTLE. Mean age at onset of the epilepsy was 15.85 years and mean duration of epilepsy was 20.28 years. All patients had been seizure-free for a minimum of 24 h prior to DTI and PET scan. PET scan was acquired within a few weeks after presurgical evaluation.

The control group for quantitative analysis of ^{18}F-FDG-PET included 30 healthy volunteers (15 women and 15 men, mean age 37.8 years ± 8.79, range 23 to 54 years) from our clinical database. For quantitative analysis of DTI, an identical DTI protocol was performed in another 30 healthy volunteers (15 women and 15 men, mean age 32.6 years ± 6.55 years, range 27 to 53 years). None of them had neurological or psychiatric disorders.

The distribution of age was not different between groups (ANOVA using IBM SPSS Statistics v19). Written informed consent was obtained from all participants, and the study was approved by our hospital's ethics committee.

2.2. Image acquisition and processing

2.2.1. ^{18}F-FDG-PET

Images were acquired in 3-dimensional mode with Siemens PET/CT Biograph equipment (Siemens, Erlangen, Germany) with an ECAT EXACT HR + BGO PET and an helicoidal CT scanner (Somatom, Emotion) for attenuation correction. Patients were required to rest quietly in a dimly lit room during the 40 min following ^{18}F-FDG intravenous administration of about 5 MBq/kg. Subsequently, 35 tomographic attenuation-corrected brain sections were obtained in all projections (2.47 mm slice thickness), using a standard 11-min routine (1 min for transmission and 10 min for emission tomography). Ordered subset expectation maximization (OSEM) algorithm (16 subsets and 6 iterations) was used for PET data reconstruction with a matrix of 128 × 128 × 64 and 2.6 × 2.6 × 2.4 mm^3 voxel size. All the patients were recorded on the same scanner. Simultaneous-EEG during FDG uptake was not performed. In order to ensure that the studies were acquired during the interictal state the patients were supervised by trained personal from our epilepsy unit at all times during the performance test. In addition, patients were requested to report whether they had experienced their typical auras/seizures during scanning.

For voxel-based analysis, data were analyzed using Statistical Parametric Mapping 8 (SPM8, Wellcome Department of Cognitive Neurology) running on Matlab 8.0. All ^{18}F-FDG-PET images, including normal control scans, were spatially normalized into an in-house ^{18}F-FDG template. This template was obtained from the PET scans of our 30 control subjects were spatially normalized to the SPM standard [15O]-H2O PET template, using the algorithm provided with SPM8. An intensity normalization was also applied to the spatially normalized studies using a previously described method (Marti Fuster et al., 2013). Then, an intermediate ^{18}F-FDG PET template was built by averaging these normalized images and applying a smoothing Gaussian filter (FWHM = 8 × 8 × 8 mm^3). To obtain a new and improved template, the above mentioned image processing procedures were repeated using the intermediate ^{18}F-FDG template in the first spatial normalization.

The regional cerebral metabolic rate of glucose utilization (rCMRGlu) of each voxel was normalized to whole brain average of rCMRGlu using a proportional scaling method provided in SPM8. Intensity-normalized images were smoothed by convolution with a Gaussian kernel of full-width-at-half-maximum (FWHM) = 8 × 8 × 8 mm^3.

2.2.2. Diffusion tensor imaging (DTI)

MRI data were acquired at 3T using a 32-channel phase array coil (Magnetom Trio Tim, Siemens Medical Systems, Germany) and parallel imaging with an acceleration factor of 2. DTI was acquired using a single-shot-echo-planar T2-weighted sequence in the axial plane with the following acquisition parameters: TR = 7600 ms; in-plane matrix 128/128; field of view 24 cm; phase of field of view 100%. DTI volumes included 82 noncollinear diffusion-encoding directions with a b-value of 1000 s/mm^2 and 6 with a b-value of 0 s/mm^2 (2-mm slice thickness and 2.5-mm isotropic resolution).

The DTI data were preprocessed in the FMRIB's Software Library (FSL) software (FSL 4.0, http://www.fmrib.ox.ac.uk/fsl). After correcting the eddy current and head motion with the affine registrations of each subject's diffusion-weighted images to the non-diffusion-weighted images in the FMRIB's Diffusion Toolbox (FDT) 2.0 (Jenkinson and Smith, 2001), the non-brain structures were removed using the Brain

Table 1
Patients' clinical information

Subject	Age (y)	Sex	Hand dominance	HS	Onset (y)/duration (y)	Seizure semiology	EEG ictal	Surgery	Surgery included ^{18}[F]-FDG-PET temporal hypometabolism	Follow-up (m)	Outcome (Engel)	Pathology
Anterior temporal hypometabolism												
1	18	M	R	L	16/2	Nonspecificaura → automotor sz	L ant T	ATR & AH	Complete	57	Ia	RA (ant), HS
2	34	F	R	L	30/4	Nonspecific aura → automotor sz (Postictal dysphasia)	L ant T	ATR & AH	Complete	41	Ic	RA (ant), HS
3	39	M	R	L	10/29	Nonspecific aura → automotor sz (Ictal speech)	L ant T	ATR & AH	Complete	12	Ia	RA (ant), HS
4	56	M	R	R	47/9	CPS/automotor sz (Postictal dysphasia)	R ant T	ATR & AH	Complete	19	Ia	RA (ant) HS
5	34	F	L	R	5/29	Psychic aura → automotor sz → GTC sz	R ant T	ATR & AH	Complete	55	Ib	RA (ant), HS
6	24	F	R	R	18/6	Automotor sz	R ant T	ATR & AH	Complete	42	Ia	CD (amygdala) & HS
7	44	F	R	R	16/28	Nonspecific aura → automotor sz → GTC sz	R ant T	ATR & AH	Complete	30	Ia	RA (ant) HS
Middle temporal hypometabolism												
8	51	F	R	L	6/45	Automotor sz (R dystonic arm; Postictal dysphasia)	L post T	No	–	–	–	–
9	60	F	L	L	3/57	Automotor sz (Postictal aphasia)	L ant/lat T	ATR & AH	Incomplete	38	Ia	CD type I (neoc) HS
10	44	F	R	L	37/7	CPS/Automotor sz → R versive → GTC sz (R dystonic arm, postictal aphasia)	L ant/lat T	No	–	–	–	–
11	39	M	L	L	20/19	CPS → complex motor sz	L ant/lat T	ATR & AH	Incomplete	47	IIIa	CD type II (neoc), HS
12	31	F	R	L	2/29	Automotor sz (Ictal speech)	L ant/lat T	ATR & AH	Complete	16	Ia	RA (ant), HS
13	34	F	R	L	30/4	Abdominal/psychic aura → CPS → GTC sz	L ant/lat T	ATR & AH	Incomplete	41	Id	CD type I (neoc) & HS
14	35	F	R	L	16/19	Nonspecific aura → automotor sz → R versive → GTC sz	L ant/lat T	No	–	–	–	–
Posterior temporal hypometabolism												
15	34	M	R & L	L	14/20	Abdominal aura → automotor sz (Postictal aphasia)	L ant/lat T	ATR & AH	Complete	46	Ia	RA (ant) HS
16	20	M	R	R	3/17	Nonspecific aura → automotor sz (Ictal speech)	R ant/lat T	ATR & AH	Incomplete	18	Ib	RA (ant) HS
17	41	F	R	R	9/32	Abdominal aura → automotor sz	R ant/lat T	ATR & AH (extended)	Complete	29	Ia	RA (ant) HS
18	33	F	R	R	9/24	CPS → GT sz (L dystonic arm, R nosewiping)	R ant/lat T	ATR & AH (extended)	Incomplete	12	Ia	RA (ant) HS
19	34	F	R	R	9/25	Abdominal aura → automotor sz	R ant/lat T	ATR & AH (extended)	Incomplete	30	Ia	RA (ant), HS
20	24	M	L	R	13/11	Abdominal aura → automotor sz (L dystonic arm)	R ant/lat T	ATR & AH	Incomplete	53	Ia	RA (ant) HS
21	30	M	R	R	20/10	Abdominal aura → automotor sz	R ant/lat T	ATR & AH	Incomplete	37	Ia	RA (ant), HS

HS, hippocampal sclerosis; Y, years; M, months; Duration, duration of epilepsy; Onset, onset of epilepsy; Follow-up, postsurgical follow-up; F, female; M, male; L, left; R, right; Ant, anterior; Lat, lateral; T, temporal; CPS, complex partial seizure; Sz, seizure; GTC, generalized tonic–clonic seizure; ATR, anterior temporal resection; AH, amygdalohippocampectomy; CD, cortical dysplasia; Neoc, neocortex; RA, reactive astrocytosis.

Extraction Tool, and the FA and MD maps were generated based on the diffusion tensors reconstructed with the DTIfit program. As a result, MD and FA maps were created in the same space as the b = 0 image volume of the original DTI acquisition.

For voxel-based analysis, data were analyzed using SPM8. The FA and MD maps were spatially normalized to a standard template using DARTEL. Prior to statistical analysis, FA and MD maps were smoothed to a Gaussian kernel of 8 mm to minimize individual variability, improve the normality of data distribution and reduce false positives.

2.3. Statistical analysis

2.3.1. Single-subject/case analysis

To investigate voxel-wise differences between each patient and the control group a two-sample *t*-test (SPM8) was performed. Age was included in the model as a nuisance variable.

For ^{18}F-FDG-PET maps significance threshold at voxel-level was set at $p < 0.001$, uncorrected. Cluster significant thresholds (extend threshold) were set at 50 contiguous voxels to reduce type I errors introduced by potential noise (Chassoux et al., 2016).

For DTI maps changes at voxel-level with $p < 0.001$ (uncorrected) were considered significant (Thivard et al., 2005). Cluster significant thresholds (extend threshold) were set at 50 contiguous voxels (Archambaud et al., 2013). Based on the results of previous studies (Dumas de la Roque et al., 2005; Gross, 2011), we selected only FA decrease and MD increase for further analysis. The results were evaluated with the Johns Hopkins University DTI WM Atlas with 50 WM tract labels (Oishi et al., 2008).

2.3.2. Group-based analysis

To investigate the relationship between ^{18}F-FDG-PET and DTI findings we first computed the differences between the FA, MD and ^{18}F-FDG-PET maps of the whole sample compared to their respective control groups. Afterward, we divided the patient group in right and left MTLE groups based on the laterality of HS and the seizure onset zone and performed a similar analysis. A two-sample *t*-test was used to investigate differences between groups. The same statistical thresholds applied for single-subject analysis were applied to group-based analysis. Disease duration was included in the model as a nuisance variable.

Lateralization indexes (LI) of the ^{18}F-FDG-PET and DTI mean significant voxels on each hemisphere were computed for the left and right MTLE groups. Asymmetries were calculated as follows (Seghier, 2008):

$$LI = \frac{LeftHemisphere - RightHemisphere}{LeftHemisphere + RightHemisphere}.$$

Laterality indices with ≥+0.1 value indicate left hemispheric lateralization and

≤−0.1 indicate rightward asymmetry, and those values between +0.1 and −0.1 represent bilateral lateralization. LI varies between −1 to +1.

For qualitative visual analysis, the FA and MD maps for whole group, left MTLE and right MTLE group analysis were overlaid on the ^{18}F-FDG-PET map (See Supplementary Fig. S1).

To assess areas of anatomical correspondence between DTI findings and ^{18}F-FDG-PET hypometabolism, we classified the main association WM tracts based on the cortical regions that they most likely connect. For that purpose, we analyzed the superior longitudinal fasciculus, the uncinate fasciculus, the inferior longitudinal fasciculus, and the cingulum. We also analyzed the corpus callosum and its connected gray matter regions in the frontal lobe (forceps minor) and in the parieto-occipital lobes (forceps major). We examined if the cortical regions connected by the selected tracts coincided with hypometabolic regions on each single-subject. To identify the tracts of interest and the cortical regions that they connected we register each single-subject FA-decrease map onto the Johns Hopkins University DTI WM Atlas with 50 WM tract labels available in the FSL software package. To identify the cortical regions that they connected we register the anatomical 3D-T1 weighted scan from each patient onto the above template. Finally, we register the PET hypometabolic findings of each subject to assess the anatomical correspondence between the FA findings and ^{18}F-FDG-PET hypometabolism. We analyzed the proportion/percentage of patients that showed coincidence of decreased FA and hypometabolism over each cortical region tract-related (See Supplementary Fig. S2).

2.3.3. Group analysis based on the extension of ^{18}F-FDG-PET hypometabolism

Based on the extension of the temporal lobe ^{18}F-FDG-PET hypometabolism, we divided the patients in anterior, middle, and posterior temporal groups. In the anterior group the hypometabolism was confined to the anterior third of the temporal lobe (3–4 cm from the temporal pole). In the middle group the metabolic deficit extended from the anterior third of the temporal lobe to an imaginary plane perpendicular to the major axis of the temporal lobe that cross through the Heschl's gyrus. The posterior group was composed for those patients whose hypometabolism extended from the anterior third of the temporal pole to beyond the imaginary plane described above. The extension of the temporal hypometabolism was visually assessed by a nuclear medicine specialist (XS) and to be included in each group at least one local maxima voxel should be present in the cluster at that location.

To analyze whether these groups differed in terms of the distribution of the microstructural abnormalities on DTI, we performed a one-sample *t*-test to determine common WM changes in each group. Resultant maps were thresholded at $p < 0.001$ (uncorrected) with an extend threshold of 50 contiguous voxels. Disease duration was included in the model as a nuisance variable.

Lateralization indexes of the ^{18}F-FDG-PET and DTI mean significant voxels were computed for the anterior and posterior temporal groups. Asymmetries were calculated as follows (Seghier, 2008):

$$LI = \frac{Anterior - Posterior}{Anterior + Posterior}.$$

We considered as “Anterior half of the brain” the frontal and temporal lobes, except for the posterior third of the temporal lobe that included in the “Posterior half of the brain”.

Laterality indices with ≥+0.1 value indicate left hemispheric lateralization and ≤−0.1 indicate rightward asymmetry, and those values between +0.1 and −0.1 represent bilateral lateralization. LI varies between −1 to +1.

2.4. Epilepsy surgery

After presurgical evaluation, 18 (86%) patients underwent epilepsy surgery. Three patients (8, 10, and 14) with left MTLE did not undergo surgery due to a high risk of memory decline.

Resections that included tissue more than 4 cm from the temporal pole were classified as extended anterior temporal lobectomy.

3. Results

3.1. Single-subject voxel-based analysis

3.1.1. ^{18}F-FDG-PET data

SPM analysis of ^{18}F-FDG-PET images showed a significant temporal hypometabolism ipsilateral to the HS in all patients. Additionally, ^{18}F-FDG-PET found extratemporal hypometabolism in all patients. Extratemporal hypometabolism was bilateral in 17 (81%) patients and ipsilateral to the seizure focus in 4 (19%) patients. The most common location of extratemporal hypometabolism was the frontal lobe (90% of patients), followed by the cingulate gyrus (86% of patients), and the insula (57% of patients). Hypometabolism was also detected in the

basal ganglia (caudate) (n = 10 (48%)), thalamus (n = 9 (43%)), mesial parietal region (precuneus) (n = 6 (29%)), and occipital inferomedial cortex (n = 6 (29%)) (For information about laterality see Supplementary Table S1).

3.1.2. DTI data

We detected widespread decreases in FA and increases in MD bilaterally (See Supplementary Table S2). The spatial pattern of WM FA and MD abnormalities varied among patients. In general, we found DTI abnormalities in WM tracts directly connected to the ipsilateral hippocampus, such as the cingulum (100%) and fornix (62%), but we also found changes in DTI parameters in closely connected tracts such as the uncinate fasciculus (67%) and the inferior longitudinal fasciculus (100%). Furthermore, we detected DTI abnormalities in WM tracts that do not originate in or pass through the temporal lobe, such as the external capsule (100%), corona radiata (100%), internal capsule (90%), and corpus callosum (100%).

3.2. Group-based voxel-based analysis

3.2.1. ^{18}F-FDG-PET data

Group analysis revealed significant hypometabolism in temporal lobes bilaterally, bilateral inferior frontal gyrus, bilateral insula, bilateral posterior cingulum/precuneus, precentral bilateral region and left angular gyrus.

Patients with left MTLE showed significant hypometabolism in the left inferior frontal gyrus, left anterior and middle temporal gyrus, left insula, left angular gyrus, left orbitofrontal cortex, left and right precentral gyrus, lent and right thalamus, brainstem, and right inferior frontal gyrus. The laterality index for this group was 0.53 indicating leftward asymmetry.

Patients with right MTLE showed significant hypometabolism mainly in the right insula, right temporal lobe, right postcentral gyrus, and right and left inferior frontal gyrus (operculum) and temporo-occipital region. The laterality index for this group was -0.34 indicating rightward asymmetry (For further details see Tables 2 and 3, and Figs. 1 and 2).

3.2.2. DTI data

Decreased FA was found in the uncinate fasciculus, inferior longitudinal fasciculus, external capsule, posterior cingulum, superior longitudinal fasciculus, anterior corpus callosum, and the corticospinal tract, bilaterally. Increased MD was found on the same WM structures as the FA had shown significant decreases.

Patients with left MTLE showed significant decreased FA in the left superior and inferior longitudinal fasciculus, left external capsule, bilateral uncinate fasciculus and left posterior cingulum/splenium. The mean decreased FA laterality index was 0.26 indicating leftward asymmetry (For further details see Table 2, and Fig. 1).

Significant increase in MD was mainly found in the left superior longitudinal fasciculus, forceps minor, inferior longitudinal fasciculus, external capsule and pyramidal tract. The mean increased MD laterality index was 0.33 indicating leftward asymmetry (For further details see Table 2, and Fig. 2).

In right MTLE patients, a significant decrease in FA was found mainly in the right inferior and superior longitudinal fasciculus, uncinate fasciculus, forceps minor, external capsule, bilateral forceps major and left uncinate fasciculus. The mean decreased FA laterality index was −0.49 indicating rightward asymmetry (For further details see Table 3, and Fig. 1).

Significant increase in MD was found mainly in the right inferior and superior longitudinal fasciculus, right uncinate fasciculus, right and left posterior cingulum and splenium of the corpus callosum. The mean increased MD laterality index was −0.28 indicating rightward asymmetry (For further details see Table 3, and Fig. 2).

After visual qualitative analysis, cortical hypometabolism was largely overlying the FA and MD changes in the temporal lobes, bilateral anterior insula, bilateral inferior frontal gyrus, bilateral precuneus and bilateral central and precentral regions (See Supplementary Table S3 and Supplementary Fig. S1).

After semi-quantitative analysis of the anatomical correspondence between DTI findings and ^{18}F-FDG-PET hypometabolism, all the subjects showed decrease FA in the inferior and superior longitudinal fasciculus, and uncinate fasciculus coincided with an overlying extensive temporal and inferior frontal gyrus PET-hypometabolism, ipsilateral to the epileptogenic foci. In addition, FA changes topographically coincided with PET-hypometabolism in the frontal lobe (forceps minor [15/21 (71.5%)]), cingulum superior projections [15/19 (78.9%)], superior longitudinal fasciculus-perisylvian region [18/20 (90%)]; parietal lobe (cingulum projections [14/21 (66%)]) and superior longitudinal fasciculus-angular gyrus [19/21 (90%)]; cingulum anterior [14/16 (87.5%)] and posterior [17/19 (89.5%)]; and occipital lobe forceps major [14/21 (66%)] and inferior longitudinal fasciculus [16/18 (88.9%)] (See Supplementary Fig. S2).

3.3. Group analysis based on the extension of ^{18}F-FDG-PET hypometabolism

Even though all the patients included in the study showed a significant anterior temporal hypometabolism, we grouped patients based on the extent of the ^{18}F-FDG-PET hypometabolism in the temporal lobe ipsilateral to the seizure onset. Seven patients were included in the anterior temporal group, 7 patients in the middle temporal and 7 patients in the posterior temporal group. We found no significant differences (Kruskal-Wallis test) in age, age at onset, or duration of epilepsy between the three groups (See Table 4 and Fig. 3). The anterior to posterior laterality index for the anterior temporal group was 0.39 indicating asymmetry in the anterior-posterior direction and for the posterior temporal group −0.04 indicating asymmetry in the anterior-posterior direction.

3.3.1. Anterior temporal ^{18}F-FDG-PET hypometabolism group

Significant decreases in FA were found in the superior longitudinal fasciculus, external capsule, uncinate fasciculus, corpus callosum (genu) and anterior cingulum, bilaterally.

Increases in MD were found on the same regions that showed FA changes. The anterior-posterior laterality index for FA decrease was 0.31 and for MD increase was 0.58 indicating asymmetry in the anterior-posterior direction (See Table 4 for further details).

3.3.2. Middle temporal ^{18}F-FDG-PET hypometabolism group

Significant decreases in FA were mainly found in the superior longitudinal fasciculus, cingulum (anterior and posterior), corpus callosum (forceps major and minor), and inferior longitudinal fasciculus. Also, corpus callosum (genu), external capsule and uncinate fasciculus showed significant increases in MD. In this particular group, DTI abnormalities predominated over the left hemisphere because all included patients had left MTLE (See Table 4 for further details).

3.3.3. Posterior temporal ^{18}F-FDG-PET hypometabolism group

Significant decreases in FA were mainly found in posterior corona radiata (precuneus), corpus callosum (splenium), posterior cingulum and superior longitudinal fasciculus, bilaterally. Increase in MD was found on the same regions that showed FA changes. The anterior-posterior laterality index for FA decrease was −0.07 indicating a trend towards an asymmetry in the posterior-anterior direction and for MD increase was −0.13 indicating a weak asymmetry in the posterior-anterior direction (See Table 4 for further details).

Table 2
Left MTLE-HS group voxel-based analysis.

^{18}F-FDG-PET hypometabolism							Decreased fractional anisotropy (FA)							Increased mean diffusivity (MD)						
Anatomical region	Cluster size (mm^3)	Cluster level p corrected	MNI coordinates			*t* statistic	Anatomical region	Cluster size (mm^3)	Cluster level p corrected	MNI coordinates			*t* statistic	Anatomical region	Cluster size (mm^3)	Cluster level p corrected	MNI coordinates			*t* statistic
			x	y	z					x	y	z					x	y	z	
L inf F g (opercular)	1325	0.05(FWE)	−50	32	14	30.61	L SLF (F)/forceps minor	24 1457	0.05(FWE) 0.001	−54	12	−4	20.08	L SLF (F)/forceps minor	1250	0.05(FWE)	−44	32	−12	13.75
L Temporal (ant & mid)	4260	0.05(FWE)	−58	6	−26	30.52	L ILF	828	0.05(FWE)	−40	16	30	13.54	L ILF	247	0.001	−48	−2	36	10.73
L Insula	648	0.05 (FWE)	32	18	2	28.35	L EC	78	0.05(FWE)	−32	60	39	14.52	L EC	89	0.001	−20	22	12	9.54
L Angular g/Lat occipital	612	0.05(FWE)	−58	−64	32	20.21	L SLF/IFL	181	0.001	−40	−62	12	8.27	L SLF/IFL	218	0.001	−34	−24	−10	7.65
R Precentral g	574	0.05(FWE)	32	−24	52	16.06	Post corona radiata/pyramidal tract	118	0.001	28	−70	28	9.77	R pyramidal tract	134	0.001	10	−36	54	7.22
R inf F g (opercular)	59	0.05(FWE)	58	34	14	15.29	R Unc	477	0.05(FWE)	18	26	−4	12.76	R Unc	289	0.001	18	30	−6	7.83
L Precentral g	621	0.05(FWE)	−52	−6	48	11.84	L SLF/pyramal tract	879	0.001	−42	−44	36	9.23	L SLF/pyramidal tract	461	0.001	−18	−10	72	10.97
L Orbito-frontal	71	0.05(FWE)	−24	40	−24	11.18	L Unc	136	0.05(FWE)	26	4	−4	14.89	L Unc	65	0.001	−18	36	−4	9.25
Brainstem	1400	0.001	4	−26	−12	10.66														
L Thalamus	681	0.05(FEW)	−18	0	2	11.28														
R Thalamus	248	0.001	4	−26	−4	9.66														
L occipital pole	183	0.001	−34	−94	−8	9.51	L IFO/ILF/forceps major	241	0.001	−28	−94	−14	8.27	L IFO/ILF/forceps major	104	0.001	−32	−78	0	7.67
L mid & post Cing	109	0.001	−6	−52	24	8.69	L Cing/CC (Splenium)/F. Major	1554	0.05(FWE)	−20	30	2	12.40	L Cing/CC (Splenium)/forceps major	737	0.001	0	−38	22	7.28
L sup F g	142	0.001	−6	60	32	8.34	Forceps minor	374	0.001	0	−38	22	7.27	Forceps minor	159	0.001	−18	32	16	5.75
R ant Temporal	83	0.001	62	4	−26	8.00	R ILF	131	0.001	56	−12	−26	11.45							
R inf F	54	0.001	42	56	12	7.39	R SLF	77	0.001	54	4	−14	10.61	R SLF/forceps minor	859	0.001	20	32	4	6.75
L Basal Ganglia (pallidum)	681	0.001	−18	0	2	11.28														
							R post Cing	174	0.001	16	−46	40	9.68	R post Cing	79	0.001	12	−40	30	5.25
							R CC/forceps major	79	0.001	24	−82	20	9.24	R CC/forceps major	65	0.001	4	−42	14	5.43

L, left; R, right; Inf, inferior; Lat, lateral; Ant, anterior; Post, posterior; Mid, middle; F, frontal; G, gyrus; T-O: temporo-occipital; Prec, precuneus; Cing, cingulum; EC, external capsule; CC, corpus callosum; Unc, Uncinate fasciculus; IFO: inferior fronto-occipital fasciculus; SLF, superior longitudinal fasciculus; ILF, inferior longitudinal fasciculus; FWE: family-wise error; MTLE, mesial temporal lobe epilepsy; HS, hippocampal sclerosis; MNI, Montreal Neurological Institute and Hospital.

Table 3
Right MTLE-HS group voxel-based analysis.

^{18}F-FDG-PET hypometabolism							Decreased fractional anisotropy (FA)							Increased mean diffusivity (MD)						
Anatomical region	Cluster size (mm^3)	Cluster level p corrected	MNI coordinates			*t* statistic	Anatomical region	Cluster size (mm^3)	Cluster level p corrected	MNI coordinates			*t* statistic	Anatomical region	Cluster size (mm^3)	Cluster level p corrected	MNI coordinates			*t* statistic
			x	y	z					x	y	z					x	y	z	
R Insula	451	0.05(FWE)	34	22	−16	17.07	R EC	120	0.001	32	14	6	10.36	R EC	144	0.001	36	6	−10	7.24
R inf F g (opercular)	318	0.05(FWE)	56	34	2	14.57	R IFO/Unc	355	0.05(FWE)	50	40	8	14.08	R IFO/Unc	256	0.001	52	20	14	7.28
L inf F g (opercular)	204	0.05(FWE)	−52	36	10	13.89	L IFO/Unc	133	0.001	−52	30	−4	10.49	L IFO/Unc	89	0.001	−53	10	20	6.27
R Temporal lobe	976	0.05(FWE)	60	2	−30	12.60	R ILF/SLF	1169	0.05(FWE)	64	−20	4	17.61	R ILF/SLF	976	0.05(FWE)	30	4	−32	12.42
R Postcentral g	68	0.001	26	−32	58	9.77	L Cortical-spinal tract	415	0.001	22	−26	48	7.25	R post Cing	65	0.001	10	−22	32	7.38
L Precentral g	36	0.001	−48	22	38	9.27	L Cortical-spinal tract	378	0.001	−24	−22	34	6,97	L post Cing	52	0.001	−8	−22	−29	7.16
R Prec/post Cing	798	0.001	14	−60	16	8.34								R Corona Radiata	258	0.001	48	−38	32	6.66
R T-O	35	0.001	58	−60	−22	7.80	R IFO/forceps mayor	516	0.05 (FWE)	20	−80	10	14.91	R CC (Splenium)/forceps mayor	148	0.001	10	−24	28	7.02
L T-O	126	0.001	−50	−76	−12	13.11	L IFO/forceps mayor	626	0.05 (FWE)	−18	−90	12	14.44	L CC (Splenium)/forceps mayor	145	0.001	−18	−44	22	7.03
														R, L CC (ant)/forceps minor	369	0.001	4	18	20	8.59
														L EC	87	0.001	−27	42	10	6.86
														L corona radiata	186	0.001	−34	−52	16	6.34

L, left; R, right; Inf, inferior; Ant, anterior; Post, posterior; F, frontal; G, gyrus; T-O: temporo-occipital; Prec, precuneus; Cing, cingulum; EC, external capsule; CC, corpus callosum; Unc, Uncinate fasciculus; IFO: inferior fronto-occipital fasciculus; SLF, superior longitudinal fasciculus; ILF, inferior longitudinal fasciculus; FWE: family-wise error; MTLE, mesial temporal lobe epilepsy; HS, hippocampal sclerosis; MNI, Montreal Neurological Institute and Hospital.

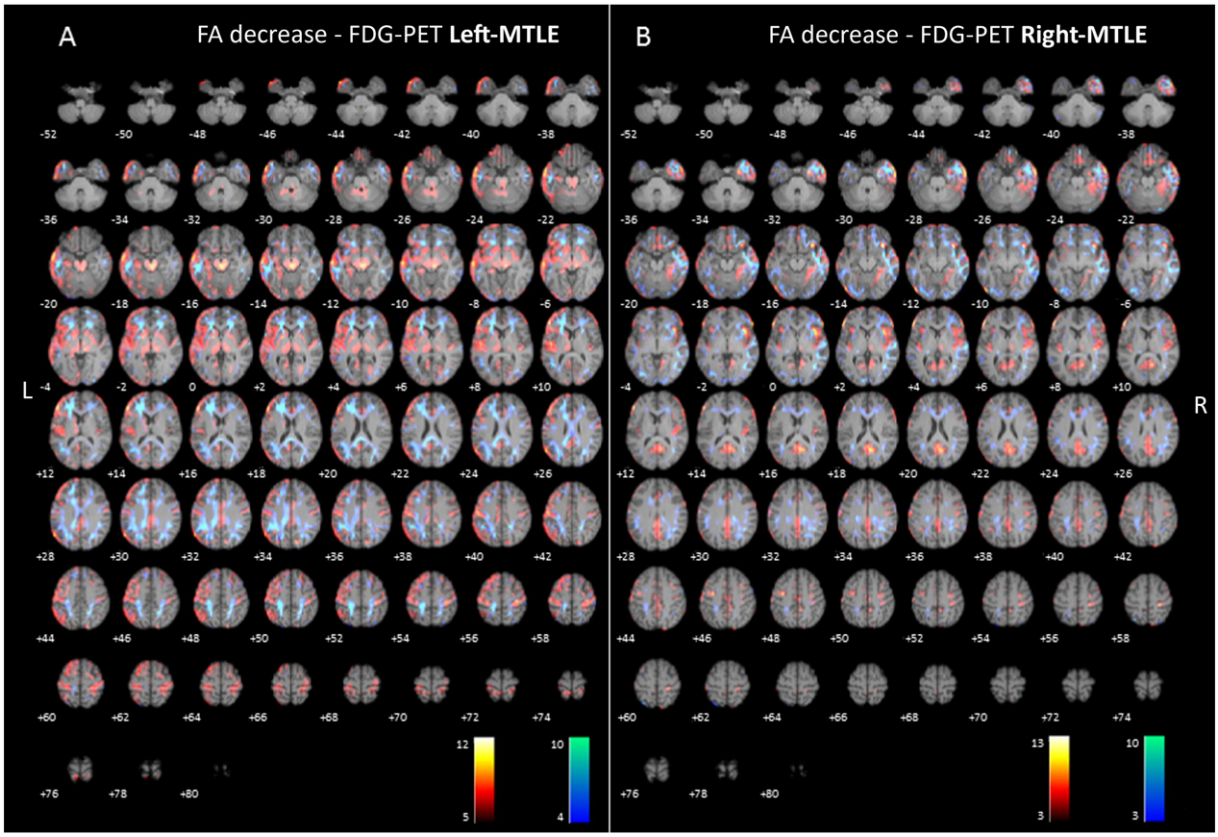

Fig. 1. (*2-column fitting image*). Axial sections of images illustrating white matter alterations (cool colors), corresponding to decreased fractional anisotropy (FA), and ^{18}F-FDG-PET hypometabolism (warm colors) in patients with left (A) and right (B) mesial temporal lobe epilepsy with hippocampal sclerosis (MTLE-HS) compared to controls. Right on image is patients' right.

3.4. Epilepsy surgery outcome

To date, 18 patients (86%) have undergone surgery. Fifteen of these underwent anterior temporal lobectomy, and three underwent extended anterior temporal lobectomies based on the extent of the hypometabolism and the ictal seizure pattern. After a mean follow–up of 36 months (range, 12–57 months), 13 (72%) patients are seizure-free (Engel class Ia); two have only infrequent psychic auras (Engel class Ib); one (patient 2) had some disabling seizures after surgery (Engel class Ic); one (patient 13) had generalized convulsions only after discontinuation of antiepileptic treatment (Engel class Id); and one (patient 11) continues experiencing seizures (Engel class IIIa).

4. Discussion

In this study, we found that patterns of white matter alterations and cortical glucose hypometabolism involved similar regions in MTLE. Although changes in DTI were more diffuse, affecting the major WM tracts related/connected to the temporal lobe, cingulum and corpus callosum, an overlap with ^{18}F-FDG-PET hypometabolism was evident over the temporal, frontal and parieto-occipital lobes. Additionally, patients with left MTLE showed more extensive metabolic and WM abnormalities than patients with right MTLE. We also found that the temporal hypometabolism pattern was not restricted to the ipsilateral anteromedial temporal lobe structures but extended contiguously into the adjacent lateral and posterior temporal lobe in two-thirds of patients. Also, the pattern of DTI abnormalities varied as a function of the extension of the temporal hypometabolism. WM abnormalities were more restricted to the anterior temporal and frontal lobes when the hypometabolism was located in anterior third of the temporal lobe and more widespread when metabolic abnormalities extended to the middle or posterior temporal lobe aspects.

Extratemporal hypometabolism was very common and usually bilateral. In agreement with previous ^{18}F-FDG-PET studies (Choi et al., 2003; Takaya et al., 2006; Wong et al., 2010), extratemporal hypometabolism most often involved the ipsilateral frontal lobe, insula, and cingulate gyrus and, less commonly, the thalamus, basal ganglia, parietal, and occipital lobe. Our results are consistent with the widespread cortical gray matter loss in temporal and extratemporal regions detected by other nonconventional neuroimaging techniques, such as quantitative structural MRI studies based on volumetry, voxel-based morphometry, cortical thickness mapping, and structural covariance (Bernhardt et al., 2010; Keller and Roberts, 2008). Although the mechanisms underlying extratemporal hypometabolism remain to be elucidated, the deleterious effect of epileptic activity propagation from the EZ through neural networks could result in cell loss and gliosis, and subsequently in metabolic disturbances (Chassoux et al., 2004; Takaya et al., 2006). Thus—as a consequence of the effect of chronic epileptic activity—, the topography of temporal and extratemporal hypometabolism might reflect the constituents of the epileptic network in MTLE. In fact, patients with left MTLE showed more extensive metabolic abnormalities than patients with right MTLE, which were more restricted to the ipsilateral hemisphere limbic structures (Hagler et al., 2009). The existence of an increased WM connectivity between the left hemisphere and the rest of the brain, probably associated with language dominance, might explain the greater involvement of the left hemisphere (Keller et al., 2002; Miro et al., 2015; Powell et al., 2006). In addition, left MTLE patients showed a marked hypometabolism over thalamus and the brainstem (Choi et al., 2003; Wong et al., 2010). Given the projections of the thalamus to the bilateral frontocentral regions, cingulate gyrus, parietal, lateral temporal and

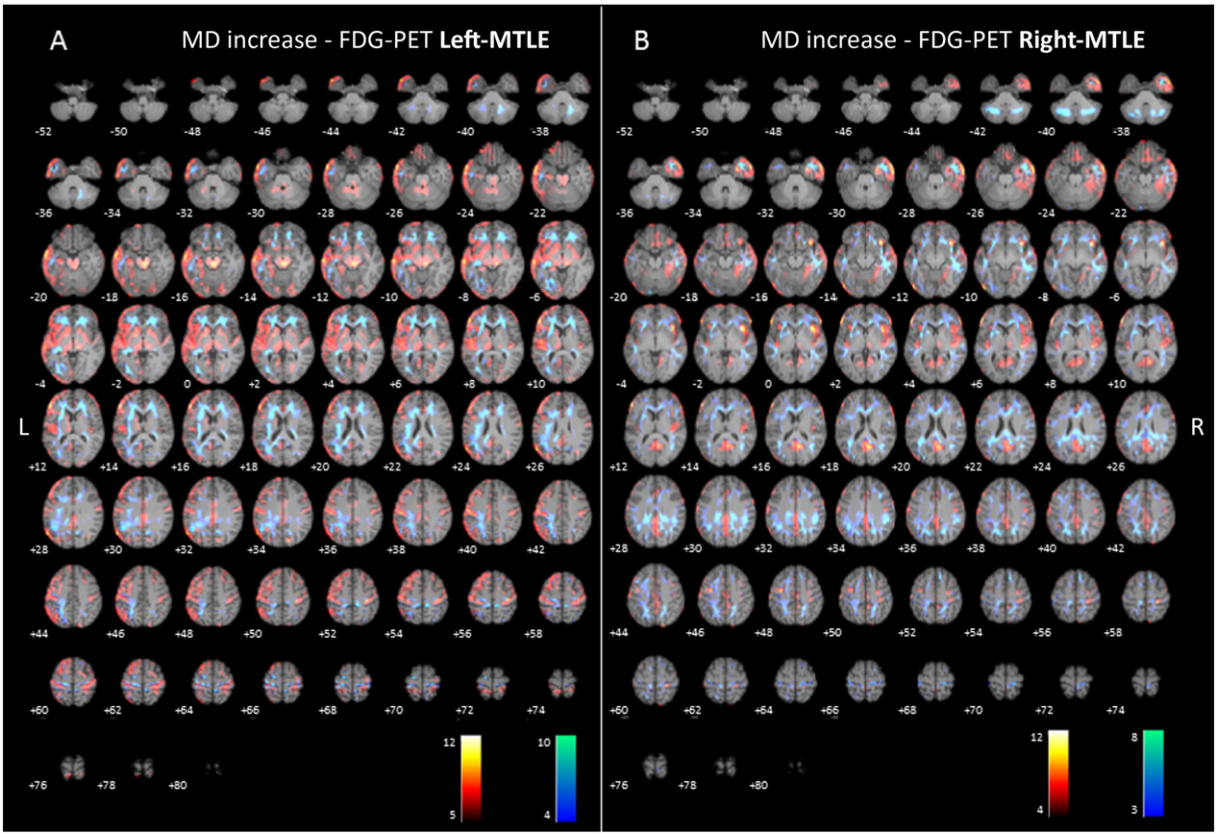

Fig. 2. (*2-column fitting image*). Axial sections of images illustrating white matter alterations (cool colors), corresponding to increased mean diffusivity (MD), and ^{18}F-FDG-PET hypometabolism (warm colors) in patients with left (A) and right (B) mesial temporal lobe epilepsy with hippocampal sclerosis (MTLE-HS) compared to controls. Right on image is patients' right.

mesiotemporal structures (Bernhardt et al., 2012; Bonilha et al., 2010), this finding could also explain the bilateral and widespread hypometabolism found in the left MTLE group compared to right MTLE group. Another difference between left and right MTLE patients was the unequal involvement of the cingulum, one of the most prominent limbic white matter tracts, both containing afferent and efferent connections to and from the hippocampus. Meanwhile patients with left MTLE showed a moderate impairment in the anterior cingulate gyrus, patients with right MTLE showed a marked involvement of the splenium bilaterally. This finding support previous evidence suggesting that networks involved in left MTLE and right MTLE are not symmetrical (Coito et al., 2015; Pail et al., 2010; Zubler et al., 2003).

Consistent with previous studies (Concha et al., 2009; Gross, 2011; Otte et al., 2012), DTI abnormalities in our study were not confined to the ipsilateral hippocampus but involved an extensive and bilateral network of WM tracts. We found decreased FA and increased MD in the bilateral limbic system (fornix, cingulum), external capsule, frontotemporal connections, temporo-occipital connections, and corpus callosum. However, as occurred with ^{18}F-FDG-PET abnormalities, the distribution of DTI abnormalities was more widespread and bilateral in left MTLE patients when compared to right MTLE patients, in line with previous studies (Ahmadi et al., 2009; Coito et al., 2015; Focke et al., 2008). Left MTLE patients tend to show a marked involvement of the corpus callosum (genu, body and splenium) that could explain the extensive diffusion changes found in the frontal and parietal WM bilaterally (Asadi-Pooya et al., 2008; Concha et al., 2009; Gross et al., 2006; Miro et al., 2015), since the corpus callosum represents the most important connection of the interhemispheric propagation of the epileptic activity, connecting both, homotopic and heterotopic cortical regions of the hemispheres. Our DTI results provide evidence that even focal epilepsy disorders, such as MTLE, are associated with highly diffuse, often bilateral, structural and functional disturbances, which could contribute to the development and maintenance of chronic epilepsy. It remains to be established whether these widespread network changes arise as a result of the same initial insult causing HS, if they are subsequent to HS, of if they arise independently (Thom, 2014).

When we compared the patterns of WM abnormalities and cortical glucose hypometabolism, at a group-level, we noticed that both involved similar brain regions. We observed that the cortical hypometabolism was largely overlying the disruption in WM integrity, bilaterally, in cingulum, external capsule, temporal, frontal and parieto-occipital lobes, in agreement with a previous study that found DTI abnormalities co-localized with PET hypometabolism in patients with TLE (Lippe et al., 2012). If we take into account that the hypometabolism involved a network of regions functionally and anatomically connected to the hippocampus, we could think that the pattern of WM changes depicted by DTI may indirectly represent the pathways/framework that coupled the hippocampus to temporal and remote extratemporal regions. In the other way, the exact physiopathology of ^{18}F-FDG-PET hypometabolism is still unknown but it seems to represent more than a functional change—potentially reversible—as it is widely associated to changes in WM microstructure—mostly permanent abnormalities (Concha et al., 2007) —related to cell loss and axonal degeneration, as shown in this study. Although we cannot draw inferences on any causal or temporal relationship between abnormalities in WM and cortical hypometabolism, our findings show evidence that microstructural changes in WM coincide with gray matter hypometabolism in a widespread network of structures linked to the hippocampus. Further longitudinal imaging studies may reveal the temporal course of WM and gray matter alterations in MTLE.

In addition, the pattern of WM diffusivity alterations found in our sample group could play a significant role in the widespread decrease

Table 4
Group analysis based on the extension of ^{18}F-FDG-PET hypometabolism

	^{18}F-FDG-PET hypometabolism								Decreased fractional anisotropy (FA)			
	Anatomical region	Hemisphere	Cluster size (mm^3)	Cluster level p corrected	MNI coordinates			*t* statistic	Anatomical region	Hemisphere	Cluster size (mm^3)	Cluster level p corrected
					x	y	z					
Anterior temporal group	Insula	L	182	0.001	−36	4	−8	15.10	EC/Uncinate/IFO/Cra	L	1101	0.05 (FWE)
		R	104	0.001	48	−6	2	12.85		R	1289	0.05 (FWE)
	Ang g/mid-inf F g	L	140	0.001	−48	20	40	12.90	SLF	L	240	0.05 (FWE)
										R	120	0.05 (FWE)
	inf F g	L	97	0.001	−4	66	−6	11.65	CC (genu)/forceps minor	L	54	0.05 (FWE)
		R	35	0.001	58	28	12	7.93		R	158	0.05 (FWE)
	Ant temp	L	141	0.05(FWE)	−64	−20	−22	16.46	ILF	L	89	0.001
		R	156	0.001	68	−30	−26	9.17		R	105	0.001
	Lingual g	L	49	0.001	−12	−58	−8	9.17	Cingulum, ant	L	102	0.05 (FWE)
		R	37	0.001	8	−58	0	8.95		R	78	0.05 (FWE)
Middle temporal group												
	Ant & Lat temp (mid)	L	3109	0.05(FWE)	−58	2	.16	32.40	ILF	L	1099	0.05 (FWE)
		R	50	0.001	64	4	−24	11.05		R	116	0.001
	Cingulum, ant	L	45	0.001	−9	19	20	10.35	Cingulum, ant/F mi	L	106	0.05 (FWE)
	Cingulum, post	L	34	0.001	−7	−37	30	9.42	Cingulum, post/F mi	L	297	0.05 (FWE)
										R	85	0.001
	Inf F g	L	358	0.001	−50	38	4	18.51	Uncinate/IFO/Cra	L	1023	0.001
		R	157	0.001	58	36	14	17.41		R	123	0.001
	Angular g	L	301	0.001	−58	−66	30	14.36	SLF	L	868	0.05 (FWE)
		R	30	0.001	16	−82	40	16.53		R	120	0.001
	Insula	L	298	0.05(FWE)	−34	18	4	19.24	EC (SLF)	L	224	0.001
	Inf occipital	L	123	0.001	−26	−98	−20	12.37	IFO, post	L	94	0.001
										R	74	0.001
	Sup-mid F g/perirol	L	636	0.001	−9	19	29	12.52	Centrum Semiovale	L	104	0.001
		R	102	0.001	36	−22	53	9.02				
	Thalamus	L	305	0.001	−16	−2	12	12.43	ALIC	L	254	0.001
	Brainstem	L	211	0.05(FWE)	−6	−18	−14	18.45		R	182	0.05 (FWE)
		R	435	0.05(FWE)	10	−28	−6	18.45				
	Caudate	L	65	0.001	−14	12	4	11.38				
Posterior temporal group	Ant & Lat temp (mid-post)	L	143	0.05(FWE)	−58	6	−24	11.19	ILF	L	144	0.001
		R	832	0.05(FWE)	60	−28	6	23.34		R	544	0.05 (FWE)
	Angular/Supramarg g	L	107	0.001	−36	−48	36	15.15	SLF	L	89	0.001
		R	65	0.05(FWE)	38	−42	34	25.90		R	435	0.05 (FWE)
	PostCentral/Sup Parietal	L	400	0.05(FWE)	−32	6	44	33.54	Cra, post/Precun	L	421	0.05 (FWE)
		R	512	0.05(FWE)	32	−22	6	30.86		R	241	0.05 (FWE)
	Inf F	L	245	0.05(FWE)	−34	54	22	20.19	Uncinate/IFO	L	208	0.05 (FWE)
		R	98	0.001	46	56	8	15.15		R	74	0.001
	Cingulum, post	L	97	0.001	−20	−66	0	13.53	Cingulum, post	L	123	0.05 (FWE)
		R	36	0.001	12	−58	10	10.36		R	102	0.05 (FWE)
	Lingual g	L	57	0.001	−13	−65	4	9.48	CC, Splenium	L	135	0.05 (FWE)
		R	128	0.001	7	−59	5	11.95		R	156	0.05 (FWE)
	Insula	R	63	0.05(FWE)	36	20	−4	10.61	EC/Uncinate	R	151	0.05 (FWE)
	Precentral	L	107	0.05(FWE)	−36	−48	36	8.06	Cra, ant	L	158	0.001
		R	104	0.05(FWE)	44	−10	34	16.36		R	102	0.001
	Temp-Occipital	L	124	0.001	−38	−88	20	16.39	IFO, F mi	L	172	0.001
		R	82	0.05(FWE)	54	−64	−10	15.26		R	251	0.05 (FWE)
	Inf F g	L	339	0.05(FWE)	−42	52	4	26.61	Cingulum, ant	L	77	0.001
		R	44	0.001	52	36	12	9.29		R	92	0.001
	Basal ganglia (Putamen)	L							CC, ant	L	65	0.001
		R	79	0.001	28	−8	0	12.09		R	145	0.001
	Thalamus	L	35	0.001	−12	18	4	8.22				
		R	54	0.001	10	−16	2	7.65				

L, left; R, right; Ant, anterior; Post, posterior; Inf, inferior; Lat, lateral; Mi, mesial; Mid, middle; G, gyrus; F, frontal; Temp, temporal; Perirol, perirolandic; Supramarg, supramarginal; Prec, precuneus; EC, external capsule; ALIC, anterior limb of internal capsule; Cra, corona radiata; CC, corpus callosum; Parahip, parahippocampus; IFO, inferior fronto-occipital fasciculus; SLF, superior longitudinal fasciculus; ILF, inferior longitudinal fasciculus; FWE, family-wise error; MNI, Montreal Neurological Institute and Hospital

Table 4 (*continued*)

	Decreased fractional anisotropy (FA)				Increased mean diffusivity (MD)							
	MNI coordinates			*t* statistic	Anatomical region	Hemisphere	Cluster size (mm^3)	Cluster level p corrected	MNI coordinates			*t* statistic
	x	y	z						x	y	z	
Anterior temporal group	−28	16	0	31.52	Uncinate/IFO/Cra	L	69	0.05 (FWE)	−34	44	−2	11.72
	28	4	−12	20.14		R	97	0.05 (FWE)	14	48	−4	12.88
	−40	−4	26	16.40	SLF	L	56	0.001	−36	−42	22	8.53
	40	−10	24	29.48		R	43	0.001	36	16	16	7.26
	−10	58	−8	17.63	CC (genu)/forceps minor	L	89	0.001	−6	28	8	9.21
	16	48	3	20.20		R	227	0.05 (FWE)	10	32	0	15.20
	−42	8	−30	11.53	ILF	L	40	0.001	−46	0	−36	6.98
	58	−4	−26	13.33		R	54	0.001	40	4	−34	7.80
	−4	18	16	17.63	Cingulum,ant	L	137	0.001	−18	46	4	7.30
	6	18	16	20.20		R	105	0.05 (FWE)	16	40	22	12.24
Middle temporal group												
	−47	17	−21	17.83	ILF	L	237	0.05 (FWE)	−34	2	40	16.49
	59	−15	−24	10.66								
	−16	27	11	16.65	Cingulum, ant/F mi	L	1204	0.05 (FWE)	−10	24	20	14.83
						R	523	0.001	12	22	22	10.94
	−14	−49	21	17.58	Cingulum, post (Prec)	L	261	0.001	−10	−60	28	10.26
	20	−46	39	6.42		R	38	0.001	6	−66	34	6.42
	−22	31	−4	10.63	Uncinate/IFO/Cra	L	2145	0.05 (FWE)	−30	44	−14	12.39
	17	27	−10	8.63								
	−38	−49	36	17.12	SLF	L	784	0.05 (FWE)	−44	−46	34	16.23
	24	−36	44	6.76								
	−33	−2	3	10.10	EC (SLF)	L	100	0.05 (FWE)	−30	0	6	18.76
	−29	−94	−14	9.18	IFO, post/F mi	L	381	0.05 (FWE)	−14	−78	4	11.30
	23	−86	18	10.21		R	117	0.001	12	−78	4	7.04
	−19	−38	53	10.67	Centrum Semiovale	L	65	0.001	−32	−34	58	6.84
	−22	27	−8	9.04	ALIC	L	130	0.05 (FWE)	−16	14	16	19.06
	20	23	3	16.97								
					CC, genu	L	258	0.05 (FWE)	−10	32	4	17.47
						R	95	0.001	4	24	2	12.76
Posterior temporal group	−26	12	−42	12.47	ILF	R	1675	0.05 (FWE)	66	−32	−4	18.40
	42	6	−34	17.93								
	−28	−34	48	9.48	SLF	L	76	0.001	−34	−60	50	10.09
	38	−54	30	18.20		R	284	0.05 (FWE)	64	−38	14	12.38
	−16	−18	38	18.59	Cra, post/Precun	L	430	0.05 (FWE)	−8	−68	36	10.46
	20	−38	38	16.67		R	358	0.05 (FWE)	12	−64	44	11.42
	−12	50	−18	18.83	Uncinate/IFO	L	178	0.05 (FWE)	−28	16	−8	13.72
	46	42	−6	11.28		R	98	0.001	16	26	−18	8.14
	−12	−42	32	18.59	Cingulum, post	L	117	0.05 (FWE)	−8	−20	34	12.18
	18	−42	32	18.20		R	672	0.05 (FWE)	6	−54	22	11.42
	−5	−21	25	18.63	CC, Splenium	L	91	0.001	−4	−34	20	9.97
	7	−25	25	17.98		R	79	0.001	4	−32	20	10.44
	36	6	−12	15.23	EC/Uncinate	L	96	0.05 (FWE)	−26	6	−2	10.49
						R	184	0.001	32	12	−2	7.05
	−26	28	46	12.06	Cra, ant	L	44	0.001	−44	16	46	9.84
	22	−24	50	11.34		R	47	0.01	8	−8	64	7.28
	−10	−104	−8	10.22	IFO, F mi/Parahip Cingulum	R	154	0.05 (FWE)	12	−84	12	20.92
	28	−98	−2	14.55								
	−10	20	22	9.29								
	14	22	22	10.34								
	−5	18	14	9.56								
	7	18	16	11.29								

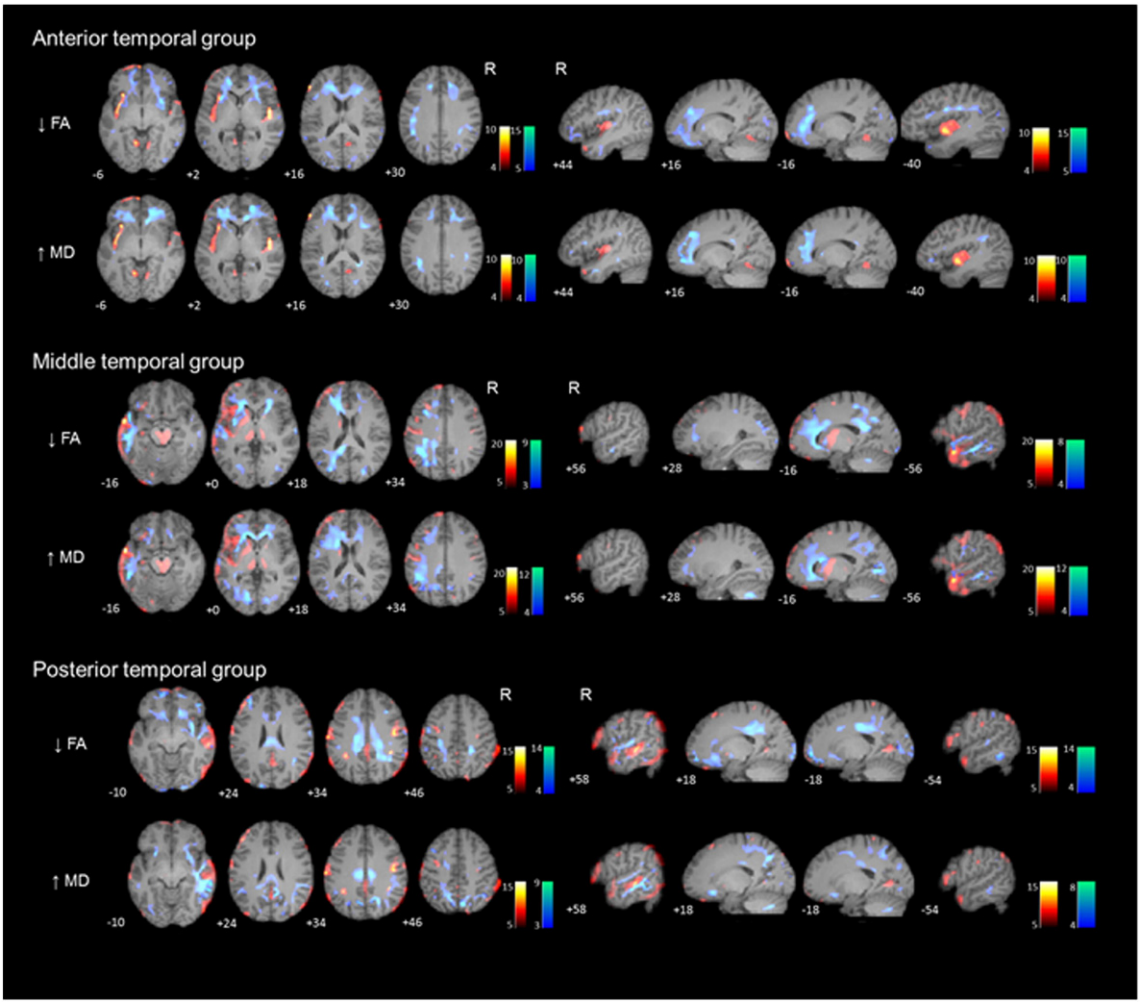

Fig. 3. (*1.5-column fitting image*). Axial (left) and sagittal (right) sections of images illustrating white matter alterations (cool colors) corresponding to decreased fractional anisotropy (FA) and to increased mean diffusivity (MD), and ^{18}F-FDG-PET hypometabolism (warm colors) in patients with mesial temporal lobe epilepsy with hippocampal sclerosis (MTLE-HS) compared to controls, based on the extension of ^{18}F-FDG-PET hypometabolism (anterior, middle and posterior groups). Numbers represent the corresponding slice. Axial images: right on image is patients' right. Sagittal images: left on image is patients' right.

in connectivity found in MTLE patients (Englot et al., 2015; Haneef et al., 2014; Voets et al., 2012). Previous studies have reported decreased connectivity in MTLE in bilateral posterior temporal and parieto-occipital cortices, perisylvian region, lateral and medial frontal neocortex, posterior cingulum/precuneus and insular cortex (Englot et al., 2015; Haneef et al., 2014; Voets et al., 2012). The decrease in connectivity may account for the deleterious effects of epilepsy including gray matter atrophy, cortical hypometabolism, neuropsychological deficits, and cognitive impairment (Thom, 2014).

We classified patients according to the extent of temporal hypometabolism on ^{18}F-FDG-PET into anterior, middle, and posterior temporal hypometabolism groups. We found WM changes on DTI in patients with anterior temporal hypometabolism differed from those in patients with middle or posterior temporal hypometabolism. Patients with only anterior temporal hypometabolism presented more restricted and anterior DTI changes—uncinate fasciculus, external capsule and corpus callosum (genu)—, whereas those with hypometabolism extending to the posterior third of the temporal lobe had more widespread DTI abnormalities involving anterior and posterior structures—superior longitudinal fasciculus, posterior cingulum, corpus callosum (splenium). To our knowledge, this is the first time that the distribution of WM changes in MTLE has been evaluated based on the extension of temporal hypometabolism. Our findings suggest that MTLE-HS is likely to be heterogeneous in terms of functional connectivity at the epileptogenic zone. However, it could be arguable that these results accrue to different patient groups (left and right MTLE) not for patterns of hypometabolism. Indeed, middle temporal hypometabolism group only contains left MTLE patients and posterior temporal group contains right MTLE except one. If this was the case the anterior temporal hypometabolism group (three patients right MTLE and four patients left MTLE) should be comprised by a mixture of left and right MTLE diffusion and hypometabolism patterns. However, the diffusion changes were very restricted to the anterior temporal and frontal lobes and the hypometabolism was very strong over the insular cortex. In fact, this insular hypometabolism could be explained due to more/stronger connections between the epileptic foci and the insula in the anterior temporal hypometabolism group compared with the middle and posterior groups. Further studies with larger number of patients are definitively necessary to elucidate whether the extent of temporal hypometabolism on ^{18}F-FDG-PET could be a useful biomarker of the extension of WM microstructural abnormalities in patients with MTLE-HS.

Strengths of this study include a well-defined cohort characterized by patients with unilateral TLE with HS confirmed by seizure freedom of at least one year after epilepsy surgery in most of them. In addition,

this study combines two neuroimaging techniques DTI and ^{18}F-FDG-PET that measures two different aspects of the pathophysiology of MTLE (structural vs. functional & white matter vs. gray abnormalities, respectively), and consequently providing complementary information. The main limitation of this study is the relatively small sample size, given the number of variables, which are relevant in this context. However, despite the modest sample size, we believe that the homogeneity in the sample recruitment allows a better understanding of the abnormalities found in ^{18}F-FDG-PET and DTI in patients with MTLE. In addition, the present study has the character of a descriptive (pilot) study, as is part of large prospective study aimed to get insight into the functional and structural changes associated to the seizure generation and propagation in patients with MTLE.

5. Conclusions

Our study in patients with MTLE-HS found widespread temporal and extratemporal ^{18}F-FDG-PET and DTI abnormalities. The pattern of WM changes was consistent with the reduction of glucose metabolism. Moreover, DTI abnormalities differed in function of the extent of the temporal ^{18}F-FDG-PET hypometabolism. These findings suggest a variable network involvement among patients with the same pathology and that the extent of temporal hypometabolism could be an indirect marker of the integrity of WM in MTLE. The use of multiple imaging modalities may improve our understanding of the anatomy of the epileptic network and may lead to a better understanding of the diffuse changes in the brain that accompany MTLE-HS.

Supplementary data to this article can be found online at http://dx.doi.org/10.1016/j.nicl.2016.05.002.

Acknowledgments

Funding was provided by grants from the Spanish Fondo de Investigaciones Sanitarias (ISCIII-MICINN), and the European Regional Development Fund (FIS-PI13/00649; PI0890278; FIS-PI080122; FIS-PI060077).

B. Martí-Fuster was awarded a PhD fellowship (App Form—Call 07-2009) from the Institute for Bioengineering of Catalonia (IBEC).

References

Ahmadi, M.E., Hagler Jr., D.J., McDonald, C.R., Tecoma, E.S., Iragui, V.J., Dale, A.M., Halgren, E., 2009. Side matters: diffusion tensor imaging tractography in left and right temporal lobe epilepsy. AJNR Am J Neuroradiol 30, 1740–1747.

Archambaud, F., Bouilleret, V., Hertz-Pannier, L., Chaumet-Riffaud, P., Rodrigo, S., Dulac, O., Chassoux, F., Chiron, C., 2013. Optimizing statistical parametric mapping analysis of 18F-FDG PET in children. EJNMMI Res. 3, 2.

Asadi-Pooya, A.A., Sharan, A., Nei, M., Sperling, M.R., 2008. Corpus callosotomy. Epilepsy Behav. 13, 271–278.

Basser, P.J., Pierpaoli, C., 1996. Microstructural and physiological features of tissues elucidated by quantitative-diffusion-tensor MRI. J. Magn. Reson. B 111, 209–219.

Bernhardt, B.C., Bernasconi, N., Concha, L., Bernasconi, A., 2010. Cortical thickness analysis in temporal lobe epilepsy: reproducibility and relation to outcome. Neurology 74, 1776–1784.

Bernhardt, B.C., Bernasconi, N., Kim, H., Bernasconi, A., 2012. Mapping thalamocortical network pathology in temporal lobe epilepsy. Neurology 78, 129–136.

Bonilha, L., Yasuda, C.L., Rorden, C., Li, L.M., Tedeschi, H., de Oliveira, E., Cendes, F., 2007. Does resection of the medial temporal lobe improve the outcome of temporal lobe epilepsy surgery? Epilepsia 48, 571–578.

Bonilha, L., Edwards, J.C., Kinsman, S.L., Morgan, P.S., Fridriksson, J., Rorden, C., Rumboldt, Z., Roberts, D.R., Eckert, M.A., Halford, J.J., 2010. Extrahippocampal gray matter loss and hippocampal deafferentation in patients with temporal lobe epilepsy. Epilepsia 51, 519–528.

Bonilha, L., Martz, G.U., Glazier, S.S., Edwards, J.C., 2012. Subtypes of medial temporal lobe epilepsy: influence on temporal lobectomy outcomes? Epilepsia 53, 1–6.

Chassoux, F., Semah, F., Bouilleret, V., Landre, E., Devaux, B., Turak, B., Nataf, F., Roux, F.X., 2004. Metabolic changes and electro-clinical patterns in mesio-temporal lobe epilepsy: a correlative study. Brain 127, 164–174.

Chassoux, F., Artiges, E., Semah, F., Desarnaud, S., Laurent, A., Landre, E., Gervais, P., Devaux, B., Helal, O.B., 2016. Determinants of Brain Metabolism Changes in Mesial Temporal Lobe Epilepsy Epilepsia.

Choi, J.Y., Kim, S.J., Hong, S.B., Seo, D.W., Hong, S.C., Kim, B.T., Kim, S.E., 2003. Extratemporal hypometabolism on FDG PET in temporal lobe epilepsy as a predictor of seizure outcome after temporal lobectomy. Eur. J. Nucl. Med. Mol. Imaging 30, 581–587.

Coito, A., Plomp, G., Genetti, M., Abela, E., Wiest, R., Seeck, M., Michel, C.M., Vulliemoz, S., 2015. Dynamic directed interictal connectivity in left and right temporal lobe epilepsy. Epilepsia 56, 207–217.

Concha, L., Beaulieu, C., Gross, D.W., 2005. Bilateral limbic diffusion abnormalities in unilateral temporal lobe epilepsy. Ann. Neurol. 57, 188–196.

Concha, L., Beaulieu, C., Wheatley, B.M., Gross, D.W., 2007. Bilateral white matter diffusion changes persist after epilepsy surgery. Epilepsia 48, 931–940.

Concha, L., Beaulieu, C., Collins, D.L., Gross, D.W., 2009. White-matter diffusion abnormalities in temporal-lobe epilepsy with and without mesial temporal sclerosis. J. Neurol. Neurosurg. Psychiatry 80, 312–319.

Dumas de la Roque, A., Oppenheim, C., Chassoux, F., Rodrigo, S., Beuvon, F., Daumas-Duport, C., Devaux, B., Meder, J.F., 2005. Diffusion tensor imaging of partial intractable epilepsy. Eur. Radiol. 15, 279–285.

Englot, D.J., Hinkley, L.B., Kort, N.S., Imber, B.S., Mizuiri, D., Honma, S.M., Findlay, A.M., Garrett, C., Cheung, P.L., Mantle, M., Tarapore, P.E., Knowlton, R.C., Chang, E.F., Kirsch, H.E., Nagarajan, S.S., 2015. Global and regional functional connectivity maps of neural oscillations in focal epilepsy. Brain 138, 2249–2262.

Focke, N.K., Yogarajah, M., Bonelli, S.B., Bartlett, P.A., Symms, M.R., Duncan, J.S., 2008. Voxel-based diffusion tensor imaging in patients with mesial temporal lobe epilepsy and hippocampal sclerosis. Neuroimage 40, 728–737.

Gross, D.W., 2011. Diffusion tensor imaging in temporal lobe epilepsy. Epilepsia 52 (Suppl. 4), 32–34.

Gross, D.W., Concha, L., Beaulieu, C., 2006. Extratemporal white matter abnormalities in mesial temporal lobe epilepsy demonstrated with diffusion tensor imaging. Epilepsia 47, 1360–1363.

Hagler Jr., D.J., Ahmadi, M.E., Kuperman, J., Holland, D., McDonald, C.R., Halgren, E., Dale, A.M., 2009. Automated white-matter tractography using a probabilistic diffusion tensor atlas: Application to temporal lobe epilepsy. Hum. Brain Mapp. 30, 1535–1547.

Haneef, Z., Lenartowicz, A., Yeh, H.J., Engel Jr., J., Stern, J.M., 2014. Network analysis of the default mode network using functional connectivity MRI in Temporal Lobe Epilepsy. J. Vis. Exp., e51442

Hemb, M., Palmini, A., Paglioli, E., Paglioli, E.B., Costa da Costa, J., Azambuja, N., Portuguez, M., Viuniski, V., Booij, L., Nunes, M.L., 2013. An 18-year follow-up of seizure outcome after surgery for temporal lobe epilepsy and hippocampal sclerosis. J. Neurol. Neurosurg. Psychiatry 84, 800–805.

Jenkinson, M., Smith, S., 2001. A global optimisation method for robust affine registration of brain images. Med. Image Anal. 5, 143–156.

Keller, S.S., Roberts, N., 2008. Voxel-based morphometry of temporal lobe epilepsy: an introduction and review of the literature. Epilepsia 49, 741–757.

Keller, S.S., Mackay, C.E., Barrick, T.R., Wieshmann, U.C., Howard, M.A., Roberts, N., 2002. Voxel-based morphometric comparison of hippocampal and extrahippocampal abnormalities in patients with left and right hippocampal atrophy. Neuroimage 16, 23–31.

Kim, Y.K., Lee, D.S., Lee, S.K., Kim, S.K., Chung, C.K., Chang, K.H., Choi, K.Y., Chung, J.K., Lee, M.C., 2003. Differential features of metabolic abnormalities between medial and lateral temporal lobe epilepsy: quantitative analysis of (18)F-FDG PET using SPM. J. Nucl. Med. 44, 1006–1012.

Lin, J.J., Riley, J.D., Juranek, J., Cramer, S.C., 2008. Vulnerability of the frontal-temporal connections in temporal lobe epilepsy. Epilepsy Res. 82, 162–170.

Lippe, S., Poupon, C., Cachia, A., Archambaud, F., Rodrigo, S., Dorfmuller, G., Chiron, C., Hertz-Pannier, L., 2012. White matter abnormalities revealed by DTI correlate with interictal grey matter FDG-PET metabolism in focal childhood epilepsies. Epileptic Disord. 14, 404–413.

Marti Fuster, B., Esteban, O., Planes, X., Aguiar, P., Crespo, C., Falcon, C., Wollny, G., Rubi Sureda, S., Setoain, X., Frangi, A.F., Ledesma, M.J., Santos, A., Pavia, J., Ros, D., 2013. FocusDET, a new toolbox for SISCOM analysis. Evaluation of the registration accuracy using Monte Carlo simulation. Neuroinformatics 11, 77–89.

McDonald, C.R., Ahmadi, M.E., Hagler, D.J., Tecoma, E.S., Iragui, V.J., Gharapetian, L., Dale, A.M., Halgren, E., 2008. Diffusion tensor imaging correlates of memory and language impairments in temporal lobe epilepsy. Neurology 71, 1869–1876.

Miro, J., Gurtubay-Antolin, A., Ripolles, P., Sierpowska, J., Juncadella, M., Fuentemilla, L., Sanchez, V., Falip, M., Rodriguez-Fornells, A., 2015. Interhemispheric microstructural connectivity in bitemporal lobe epilepsy with hippocampal sclerosis. Cortex 67, 106–121.

Oishi, K., Zilles, K., Amunts, K., Faria, A., Jiang, H., Li, X., Akhter, K., Hua, K., Woods, R., Toga, A.W., Pike, G.B., Rosa-Neto, P., Evans, A., Zhang, J., Huang, H., Miller, M.I., van Zijl, P.C., Mazziotta, J., Mori, S., 2008. Human brain white matter atlas: identification and assignment of common anatomical structures in superficial white matter. Neuroimage 43, 447–457.

Otte, W.M., van Eijsden, P., Sander, J.W., Duncan, J.S., Dijkhuizen, R.M., Braun, K.P., 2012. A meta-analysis of white matter changes in temporal lobe epilepsy as studied with diffusion tensor imaging. Epilepsia 53, 659–667.

Pail, M., Brazdil, M., Marecek, R., Mikl, M., 2010. An optimized voxel-based morphometric study of gray matter changes in patients with left-sided and right-sided mesial temporal lobe epilepsy and hippocampal sclerosis (MTLE/HS). Epilepsia 51, 511–518.

Powell, H.W., Parker, G.J., Alexander, D.C., Symms, M.R., Boulby, P.A., Wheeler-Kingshott, C.A., Barker, G.J., Noppeney, U., Koepp, M.J., Duncan, J.S., 2006. Hemispheric asymmetries in language-related pathways: a combined functional MRI and tractography study. Neuroimage 32, 388–399.

Seghier, M.L., 2008. Laterality index in functional MRI: methodological issues. Magn. Reson. Imaging 26, 594–601.

Takaya, S., Hanakawa, T., Hashikawa, K., Ikeda, A., Sawamoto, N., Nagamine, T., Ishizu, K., Fukuyama, H., 2006. Prefrontal hypofunction in patients with intractable mesial temporal lobe epilepsy. Neurology 67, 1674–1676.

Thivard, L., Lehericy, S., Krainik, A., Adam, C., Dormont, D., Chiras, J., Baulac, M., Dupont, S., 2005. Diffusion tensor imaging in medial temporal lobe epilepsy with hippocampal sclerosis. Neuroimage 28, 682–690.
Thom, M., 2014. Review: hippocampal sclerosis in epilepsy: a neuropathology review. Neuropathol. Appl. Neurobiol. 40, 520–543.
Vielhaber, S., Von Oertzen, J.H., Kudin, A.F., Schoenfeld, A., Menzel, C., Biersack, H.J., Kral, T., Elger, C.E., Kunz, W.S., 2003. Correlation of hippocampal glucose oxidation capacity and interictal FDG-PET in temporal lobe epilepsy. Epilepsia 44, 193–199.
Voets, N.L., Beckmann, C.F., Cole, D.M., Hong, S., Bernasconi, A., Bernasconi, N., 2012. Structural substrates for resting network disruption in temporal lobe epilepsy. Brain 135, 2350–2357.
Wong, C.H., Bleasel, A., Wen, L., Eberl, S., Byth, K., Fulham, M., Somerville, E., Mohamed, A., 2010. The topography and significance of extratemporal hypometabolism in refractory mesial temporal lobe epilepsy examined by FDG-PET. Epilepsia 51, 1365–1373.
Zubler, F., Seeck, M., Landis, T., Henry, F., Lazeyras, F., 2003. Contralateral medial temporal lobe damage in right but not left temporal lobe epilepsy: a (1)H magnetic resonance spectroscopy study. J. Neurol. Neurosurg. Psychiatry 74, 1240–1244.